

Polarization Dependent Effects of Radiation on Wavelength Division Multiplexers

Roman C. Gutierrez, Gary M. Swift, Serge Dubovitsky, Randall K. Bartman,
Charles L. Barnes, Leonard Dorsky
Jet Propulsion Laboratory, California Institute of Technology
4800" Oak Grove Dr., Pasadena, CA 91109

ABSTRACT

The effects of radiation on fused biconical taper wavelength division multiplexers are presented. The polarization sensitivity of these devices before and after irradiation is discussed. Preliminary results on the effects of irradiating different regions of the device, and comparisons between the effects of proton and Co^{60} radiation sources are also given. A theoretical model that takes into account the index change in the Ge-doped cores of the optical fibers used to make these devices agrees well with experimental observations. This indicates that index changes in the fiber may be primarily responsible for the effects of radiation on these devices.

Keywords: space radiation, fused biconical taper, wavelength division multiplexer, WDM, polarization, isolation

1. INTRODUCTION

Numerous articles [15, 16, 26] discuss the advantages of wavelength multiplexing in optical systems. Much the same as frequency multiplexing in radio and television, wavelength multiplexing increases the bandwidth of an optical system by the number of different wavelengths used. The combination and separation of the different optical wavelengths is performed by devices called wavelength division multiplexers (WDMs).

Several authors have studied the effect of radiation on different types of optical couplers [10-12, 24]. In this paper, we will limit ourselves to the fused biconical tapered WDM which is made by fusing together two single mode fibers. Fused biconical taper WDMs are the most widely used type of coupler in the telecommunications industry, making them the most likely candidate for multiplexed high data-rate optical buses in space.

The severe requirements for optical WDMs (30-35 dB isolation) in most telecommunications applications are barely met by fused biconical taper WDMs (typically in concatenated structures or followed by wavelength filters) [26]. In order to use these devices in space applications, the radiation hardness of these devices needs to be studied in order to establish the effects of radiation, the mechanism responsible for the effects, and possible directions to take in the development of a radiation hardened WDM.

This paper assumes a basic knowledge of WDMs. Some of the terminology applicable to these devices and a description of a fused biconical taper WDM will be included in the first section. The second section will describe the experimental procedure used to test these devices in a radiation environment. Then, a section on experimental results will outline some of the more significant results of our experiments, focusing on the polarization sensitivity measurements before and after irradiation. The remainder of the paper will present a theoretical model that attributes the observed radiation effects to changes in the index of refraction of the cores of the optical fibers comprising the WDM. This paper will modify the existing theoretical analysis of fused biconical tapered couplers [17-23, 26] to correct for core index of refraction and combine with known effects of radiation on optical fiber [1-5, 25] to predict the effects of radiation on these devices. The polarization sensitivity of these devices before and after irradiation will also be studied in some detail. Finally, the theory and the experiment will be compared.

2. WAVELENGTH DIVISION MULTIPLEXER (WDM)

A beam of light can be separated into its spectral components by many different methods, such as using gratings or prisms. Wavelength division methods such as these have been integrated with fiber and used for wavelength division multiplexing [15, 16, 24], but the most successful WDM has evolved from tapered fiber technology.

2.1 Tapered optical fiber

When an optical fiber is heated above the glass softening point and stretched symmetrically, the diameter of the fiber is decreased at the heat source and gradually tapers to the original diameter away from the heat source. When light is launched

into the tapered fiber, the mode in the fiber will change along the taper. Far away from the tapered region, the light in the fiber is guided by the core, and the cladding can be assumed to extend to infinity. But as the fiber gets thinner, the mode field diameter approaches the diameter of the cladding and the cladding becomes the guiding medium. If the taper is slow (adiabatic approximation) all the energy will be carried by the lowest order mode at every point in the fiber. In this case, there is no loss of energy and the presence of the taper is not detectable from the properties of the fiber. If the taper is very sudden, higher order modes will be excited as the light travels along the taper-down region and interfere when they couple into the fundamental mode of the fiber in the taper-up region. The so-called Stewart-Love limit [26] determines the slope of the taper below which only the fundamental mode carries the energy and above which higher order modes are excited.

2.2 Fused biconical taper WDM

When two fibers are heated and stretched together in such a way that the taper slope is below the Stewart-Love limit, the first two lower order modes are excited in the region between the tapers. The coupling between the two fibers is then determined by the interference between these two modes.

Figure 1 shows a fused biconical tapered coupler. The fused region is typically about 3 cm long, but the region where most of the coupling takes place (the coupling region in figure 1) is only around 5 mm long. The original core diameter and cladding diameters for SMF28 fiber (which is usually used to make these devices) are $9\text{ }\mu\text{m}$ and $125\text{ }\mu\text{m}$ respectively. The width of the coupling region is typically around $30\text{ }\mu\text{m}$ but varies between individual devices.

The principal coupling mechanism in fused biconical tapered couplers is fundamentally different from polished fiber-optic WDMs or optoelectronic directional couplers which work by evanescent coupling [6,7,11-13]. In a fused biconical taper coupler, most of the coupling results from the interference between the first two fundamental modes in the coupling region, which can be approximated as a rectangular waveguide of constant cross-section. Only a small portion of the coupling is evanescent.

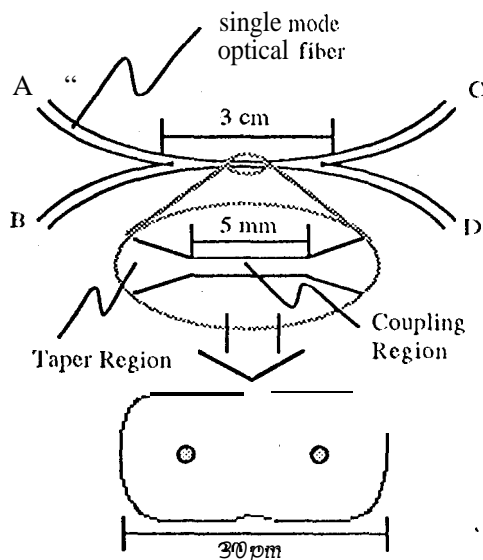


Fig. 1 A fused biconical taper WDM. Magnification and cross-section of the coupling region.

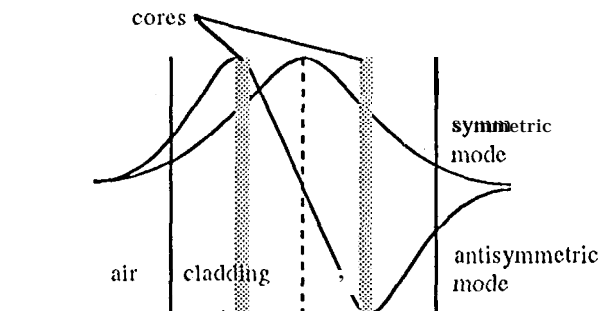


Fig 2 Side view of coupling region. Symmetric and antisymmetric mode profiles are shown.

Outside the fused region, the interaction between the two fibers is small enough that any mode can be expressed as a vector sum of the fundamental modes of the two fibers. Along the taper-down region, the modes in the two fibers begin to interact becoming distorted. This interaction results in a small amount of coupling. Since the interaction between the two modes comes from the overlap of one of the modes with the evanescent field of the other mode, this type of interaction and the energy exchange between the two modes is called evanescent coupling.

As the mode field diameter approaches the diameter of the cladding, the cores of the fibers are no longer guiding the light, and the cladding becomes the guiding structure. Since the taper slope is below the Stewart-Love limit, only the first two fundamental modes of the cladding-air waveguide are excited. These two modes are shown in figure 2.

Since the symmetric mode is more confined to the fiber than the antisymmetric mode, the antisymmetric mode propagates faster. The difference in velocity of the two modes results in a buildup of the relative phase between them as they propagate through the coupling region. As the fibers taper out, the modes adiabatically conform to the modes of the two single mode fibers forcing the symmetric and antisymmetric modes to interfere. The output of the two fibers is then determined by the interference pattern. If we ignore the phase shift between the symmetric and antisymmetric modes acquired in the tapered regions, and only consider the phase shift between the two modes in the coupling region, the coupling constant is given by:

$$C = k_S - k_A = \frac{2\pi}{\lambda} (n_S - n_A) \quad (1)$$

where n_A and n_S are the effective indices of refraction in the coupling region for the antisymmetric mode and the symmetric mode respectively. λ is the free space wavelength of light.

Due to the dependence on wavelength of the coupling constant C (n_A and n_S are also dependent on λ), fused biconical tapered couplers can be tailored to have near 100% coupling at one wavelength and near 0% coupling at a second wavelength. A coupler which is tailored in this way is called a WDM.

2.3. Terminology

In order to quantify the performance of a WDM, two figures of merit are typically used: isolation and excess loss. In figure 2, the four fibers of the WDM are labeled: A and B are the two input fibers; C and D are the two output fibers. Isolation is defined as the ratio of the output of port D to the output of port C when light at a single wavelength is injected into port A. Excess loss is the ratio of the total output to the total input. These values are usually expressed in dB.

$$\text{isolation} = 10 \log_{10} \left(\frac{I_D}{I_C} \right) \quad (2)$$

$$\text{excess loss} = 10 \log_{10} \left(\frac{I_C + I_D}{I_A + I_B} \right) \quad (3)$$

where I_A, I_B, I_C, I_D are the optical intensities at ports A, B, C, and D respectively. C is the coupling constant as given by equation (1). In addition to the isolation and the excess loss, the operating wavelength range is usually specified (typically ± 20 nm).

| Device Name | RADIATION | | | ISOLATION (dB) | | | |
|-------------|-----------|------|-----------|---|---|---------|-----------------------|
| | where | Type | Dose Mrad | $\lambda = 1.31 \mu\text{m}$ Pre-rad Δ_{rad} | $\lambda = 1.55 \mu\text{m}$ Pre-rad Δ_{rad} | Pre-rad | Δ_{rad} |
| ML-1 | whole | p+ | 1 | -19 | +3 | -28 | +10 |
| ML-2 | " | Co60 | 0.1 | -24 | +0.8 | -23.6 | +0.5 |
| " | " | " | 0.9 | -23.2 | +2.7 | -23.1 | +1.6 |
| " | " | p+ | 0.5 | -21.8 | +1.4 | -22.4 | +2.2 |
| ML-3 | input | " | 0.2 | -27.45 | 0 | -26.7 | 0 |
| " | output | " | " | -27.5 | 0 | -26.7 | 0 |
| " | center | " | " | -27.4 | -1.4 | -26.7 | -0.3 |
| " | o-c | " | " | -28.6 | -0.7 | -26.9 | -0.2 |
| " | i-c | " | " | -29.1 | -0.3 | -27.1 | -0.2 |
| Gould-1 | whole | " | 0.1 | -20.6 | +0.5 | -19.9 | +1.1 |
| " | " | " | 0.9 | -20.1 | +1.7 | -18.8 | +2.3 |
| Gould-2 | " | Co60 | 0.1 | -24.4 | -1.5 | -24 | +1.8 |
| " | " | " | 0.9 | -25.8 | -2.2 | -22.3 | +2.7 |
| " | " | " | 1 | -27.44 | -0.42 | -20.1 | +0.8 |
| " | " | " | " | -27.84 | -0.28 | -18.83 | +0.6 |
| Gould-3 | " | " | " | -25.7 | +2.4 | -25.2 | +3.9 |
| Gould-4 | " | " | 0.1 | -24.6 | +0.7 | -19.2 | +0.9 |
| " | input | " | 0.2 | -23.9 | +0.9 | -18.3 | +0.3 |
| " | output | " | " | -23 | +0.05 | -18 | 0 |
| " | center | " | " | -22.95 | +0.8 | -18 | +0.5 |
| " | whole | " | " | -22.15 | +0.45 | -17.5 | +0.3 |
| I-1 (y) | " | " | 1 | -30.7 | +5.6 | -18.5 | +2 |
| (x) | " | " | " | -33.2 | +6 | -27 | +3.5 |

Table 1. Summary of test results.

3. EXPERIMENTAL PROCEDURE

Table 1 lists all the devices that were irradiated in the order that the irradiations were performed. A description of the radiation they were exposed to is listed in the three columns labeled "RADIATION". The "where" column indicates which section of the device was irradiated. "whole" means that the entire WDM was exposed to radiation, "input" means that only a section of the WDM on the side of the input was irradiated, "output" means that a region close to the output of the WDM was exposed to radiation, "center" means that only the region in the middle of the WDM was irradiated, "o-c" stands for output-center, and "i-c" stands for input-center. The "Type" column indicates whether the device was exposed to protons (p+) or Radioactive Cobalt (Co^{60}). The "Dose" column indicates the dose received by the device in Mrad (SiO_2). The type of device tested is given in the "Device Name" column.

The ML devices were supplied by NCCOSC Research, Development, Test and Evaluation Division. These devices were bare, i.e. the taper region of the WDMs was exposed to the atmosphere. The devices were supplied in this way to permit low energy proton irradiation (6 MeV). A total of three of these devices were irradiated. The first one (ML-1) was exposed to 6 MeV protons at a dose rate of 1.3 krad/min

for the first 100 krad, and at a dose rate of 10 krad/min for the last 900 krad. ML-2 was exposed to Co^{60} for a total dose of 1 Mrad and 6 MeV protons for 500 krad. The relaxation of the device was observed for 45 minutes after 100 krad and for 9 hours after 1 Mrad. The dose rate was 1.3 krad/min for the first 100 krad and 3 krad/min for the '900 krad. The dose rate during proton irradiation was 10 krad/min. The last of these devices (ML-3) was subjected to sectional proton irradiation (5 mm sections of the device were irradiated consecutively). The dose rate was 10 krad/min. The device was masked with a 5 mm slit in a piece of aluminum.

The Gould devices were supplied by Gould inc. Fiber-Optics Division. Gould-1 and Gould-2 are the 16 dB isolation in a 40 nm band model, and Gould-3 and Gould-4 are the 10 dB isolation in a 40 nm band model. Gould-J was the only Gould device irradiated with protons. Since the devices were all packaged, the proton irradiation was done at the UC Davis Cyclotron accelerator where 60 MeV proton energy was used. The device received 100 krad at a dose rate of 1.3 krad/min and 900 krad at a dose rate of 13 krad/min. Gould-2 was exposed to Co^{60} , receiving a total dose of 3 Mrad at a dose rate of 3 krad/min. The irradiation was stopped for 1 hour after 100 krad to observe relaxation. Relaxation was observed for 9 hours after 1 Mrad, for 15 hours after 2 Mrad and for 12 hours after 3 Mrad. Gould-3 received a dose of 1 Mrad at a dose rate of 3 krad/min and was observed for 14 hours of relaxation. Gould-4 was tested for sectional Co^{60} irradiation (12.7 mm sections of the device were irradiated consecutively). The device was masked by 10 cm thick lead bricks with a 12.7 mm slit between them.

The E-1 device was supplied by ETEK Dynamics Inc. E-1 was exposed to Co^{60} receiving a dose of 1 Mrad at a dose rate of 3 krad/min. The relaxation of the device was observed for 12 hours.

The test apparatus used for in-situ measurements of the isolation and excess loss of the WDMS was modified and improved between tests. Figure 3 shows a diagram of the experimental setup used. The lasers were changed to cooled power stabilized laser diodes after the first test. ML-1 was the first device that was tested, and laser diodes at 1300 nm and 1547 nm were used. All of the other devices except for the ETEK were tested at 1306 nm and 1547 nm. The ETEK device was only tested in-situ at 1547 nm. Measurements at 1306 nm for the ETEK device were made only before and after irradiation. The laser intensity used varied from 1 μW to 100 μW . Enhanced annealing was not observed in photo bleaching tests at 1 mW optical power at both wavelengths for ML-2.

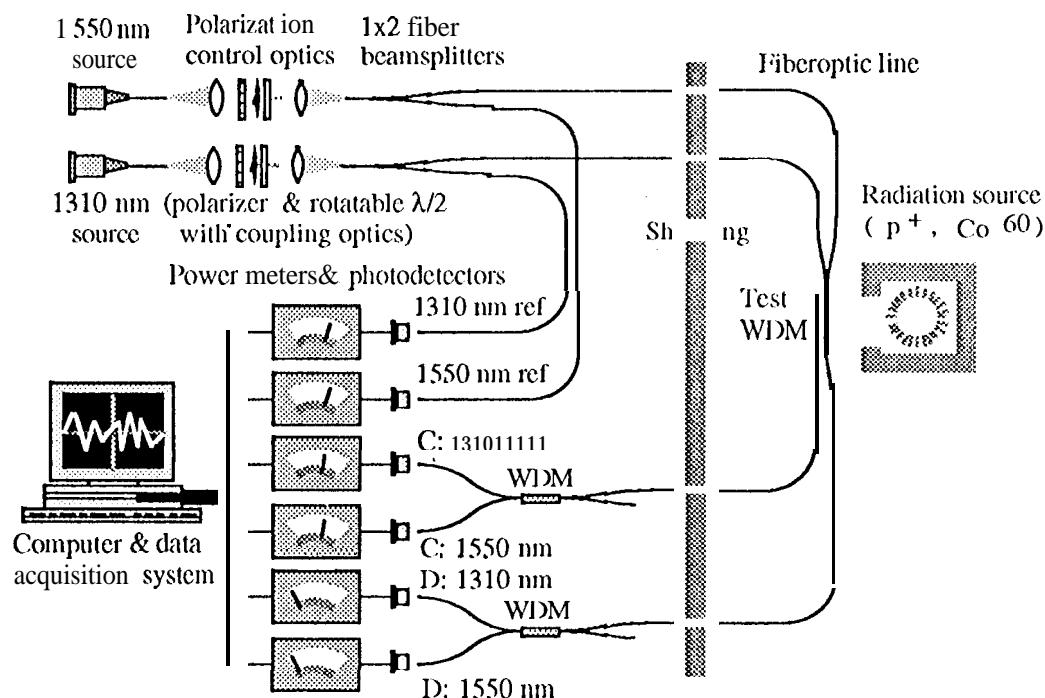


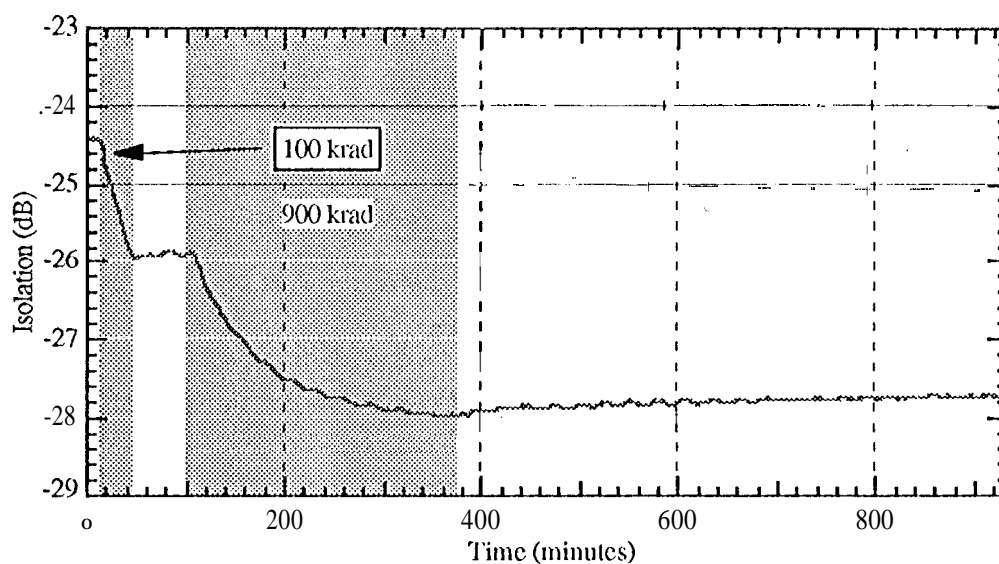
Fig. 3 Diagram of the experimental method used.

One major modification that was made after all the ML devices and the first Gould device were tested was to add polarization control to both wavelengths. The polarization control optics is shown in figure 3. It consisted of a polarizer and a $\lambda/2$ waveplate to rotate the polarization with AR coated 10X lenses to go from fiber into free-space optics and back into fiber.

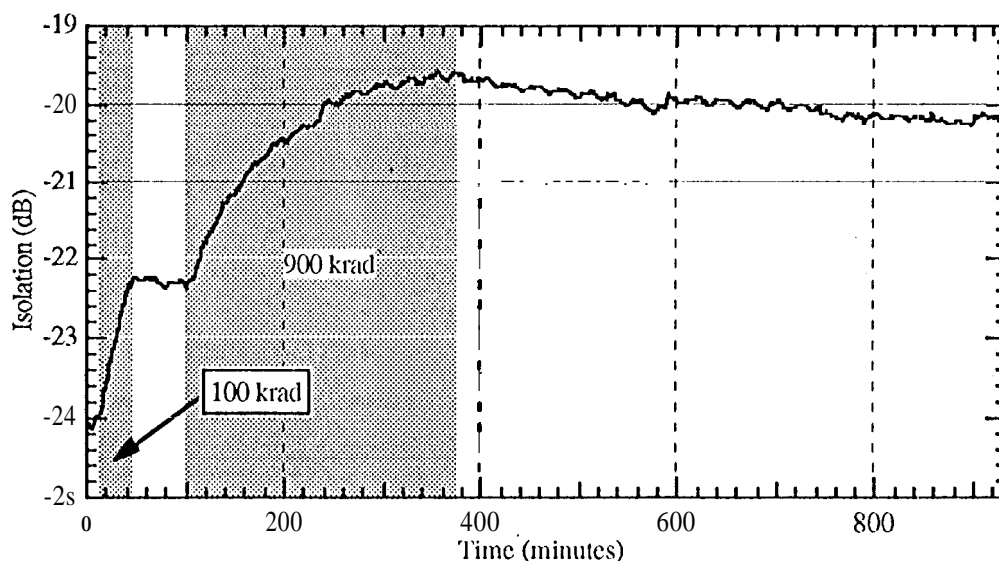
At 1547 nm, a motorized rotation stage was used to rotate a half-wave plate. At 1306 nm a manual rotation stage was used. This allowed us to measure, in-situ, the polarization properties of the WDM at 1547 nm, and to measure the polarization properties of the WDM at 1306 nm before and after irradiation.

Figure 3 illustrates the method used in these experiments to be able to measure isolation and excess loss simultaneously at two wavelengths. Light at 1310 nm is injected into one of the input fibers of the test WDM, and light at 1550 nm into the other. The test WDM is then used as a multiplexer and combines most of the light at both wavelengths into one of the output fibers. The remaining light at 1310 nm and 1550 nm comes out of the other output fiber. Two WDMs are used to demultiplex the two wavelengths at each of the output fibers of the test WDM. Six optical power sensors are used to track the two reference fibers and the four outputs of the WDM (two at each wavelength).

A measurement resolution in the crosstalk better than 0.01 dB was achieved by averaging over ten evenly spaced polarization states once the polarization control was in place.



(a)



(b)

Fig. 4 Isolation changes with radiation (gray areas) and relaxation (white runs) for Gould-2 at (a) 1306 nm and (b) 1547 nm.

4. EXPERIMENTAL RESULTS

4.1. WDM Isolation and Excess Loss

Table 1 gives the measured isolation before irradiation and the change induced by the radiation for all the tests that were done under the four columns labeled "ISOLATION (dB)". The change in isolation is given under the columns labeled " Δ rad". The principal effect of radiation on the WDMs that were tested was to change their isolation. No significant changes in the excess loss of the device were observed. (Resolution in the measurement of the output of the WDM was better than 0.1 dB.).

The most important result from our experiments is that devices cannot be directly compared. Even the Gould devices, which were matched in isolation to better than 0.5 dB at 1311 nm and 1553 nm by the manufacturer, had different isolations at our wavelengths (1306 nm and 1547 nm) and had radically different isolation changes with radiation (see Table 1). The largest change in isolation was on MI-1 which changed by 10 dB at 1547 nm after 1 Mrad of 6 MeV protons. The isolation was observed to improve for MI-3 at both wavelengths and for Gould-2 at 1310 nm.

Figure 4 shows a sample of the data that was recorded. This data is for Gould-2 and shows the improvement in isolation at 1306 nm. The shaded regions mark the time when the radiation source was exposed. The white regions show the annealing in isolation after radiation.

The results from relaxation observations are, qualitatively, the same in all of the devices that were tested. Qualitatively, they are also consistent with annealing of attenuation for SMF28 fiber [3]: less than 20 % of the total change in isolation annealed with a time constant of a few hours.

4.2. Sectional Irradiations

Sectional irradiations of MI-3 and Gould-4 give preliminary results on a very important type of experiment. Irradiating different portions of the same WDM consecutively gives information about the sensitivity to radiation of the different regions of the device. It is observed that the center region is most sensitive, and that the input and output regions are only sensitive when close to the center of the device (see MI-3). This is to be expected since the majority of the coupling takes place in a 5 mm section at the center of the device (as described in section 2.2). The fact that sections of the input and output taper regions are also somewhat sensitive to radiation seems to support the theory that some of the coupling takes place in these regions.

Figure 5 shows the results of consecutive sectional irradiations on Gould-4. The whole device was irradiated at the beginning and at the end to try to compensate for the saturation of the radiation effects on isolation. The device was packaged, so the actual location of the coupling region within the package was not known. It is apparent from the results that it is probably located closer to the input since this section is affected more strongly by the radiation than the output. These results, and results of future experiments will contribute to achieving a better understanding of the physical mechanisms that result in an interaction between radiation and the electric fields in a WDM.

4.3. Polarization Sensitivity

The first experiment to determine polarization sensitivity of these devices, was to measure the polarization dependence of isolation and excess loss for MI-2 at 1300 nm. A variation in isolation of 4 dB was measured as the polarization was changed!. This experiment verified our suspicions that isolation measurement instability is a result of the polarization sensitivity of these devices. It is therefore important to control the state of polarization when using fused biconical taper WDMs, or to at least be aware of the noise that may result if the polarization is not controlled. A means to measure the effects of radiation on the polarization sensitivity of a WDM was found and implemented starting with Gould-2.

| Device Name | 1306 nm Pre-rad Δ Isolation p/p | 1306 nm Post-rad Δ Isolation p/p | 1547 nm Pre-rad Δ Isolation p/p | 1547 nm Post-rad Δ Isolation p/p |
|-------------|---|--|---|--|
| Gould-2 | 0.22 dB | 0.25 dB | 0.11 dB | 0.11 dB |
| Gould-3 | 0.75 dB | 0.85 dB | 1.1 dB | 0.45 dB |
| Gould-4 | 1.41 dB | 1.15 dB | 0.54 dB | 0.37 dB |
| ETEK-1 | 2.5 dB | 2.2 dB | 8.5 dB | 7.5 dB |

Table 2. Summary of results of polarization measurements before and after total radiation received by each device.

Table 1 includes the dependence on polarization for the ETEK device, which was found to be very sensitive to polarization. The x and y polarizations are shown. The x polarization has an electric field which is only appreciable on the plane on which the cores of the two fibers lie, and the y polarization has an electric field on a plane orthogonal to the other plane that is parallel to and equidistant from the cores of the two fibers.

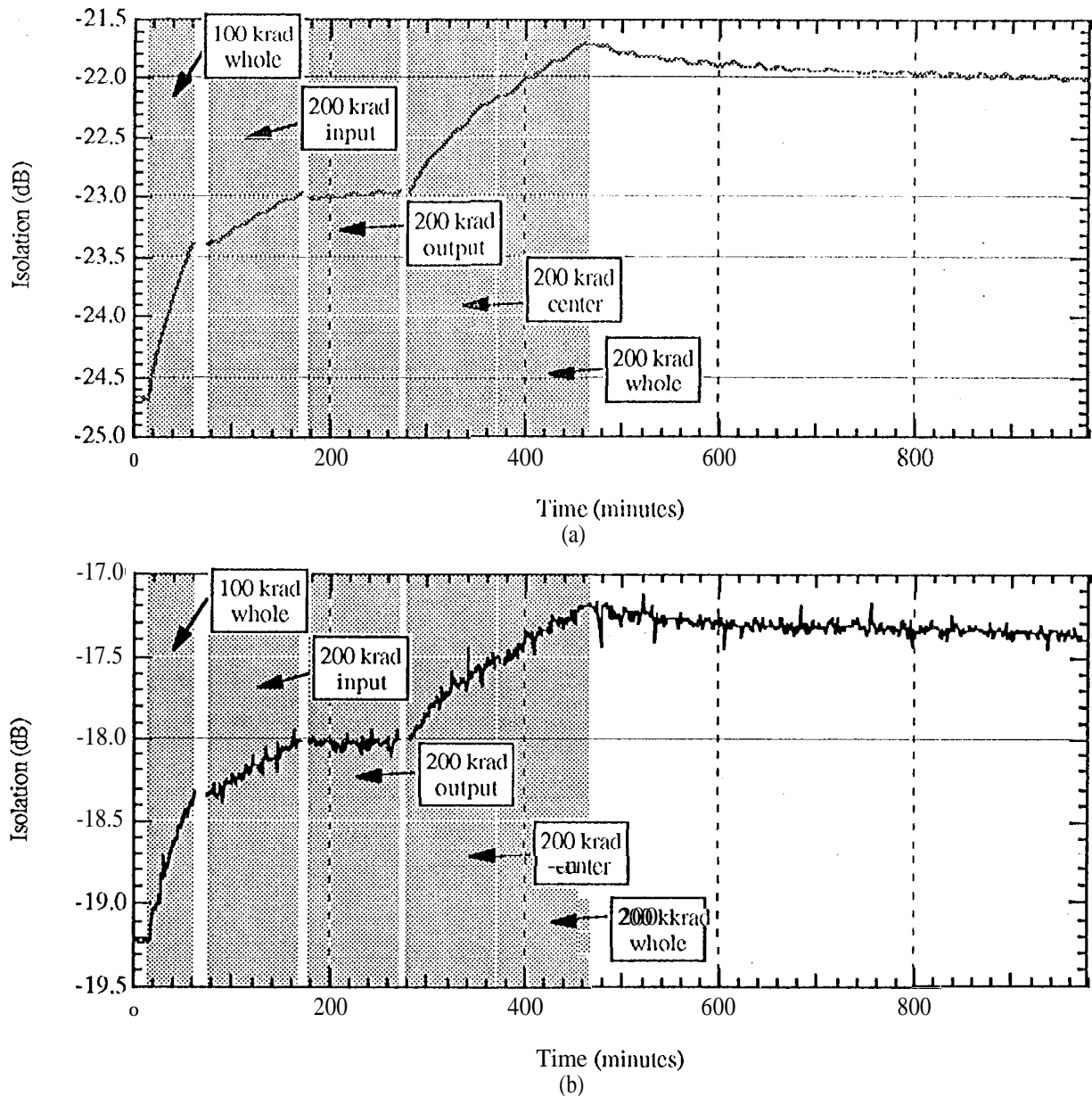
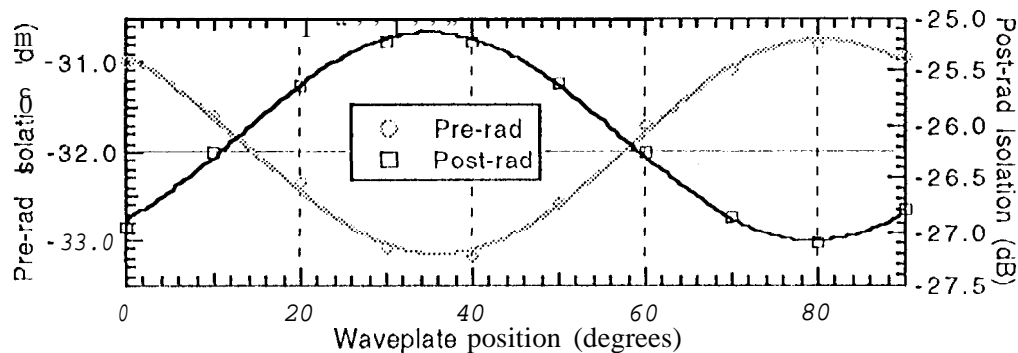


Fig. 5 Isolation changes with radiation (gray areas) and relaxation (white areas) for Gould-4 at (a) 1306 nm and (b) 1550 nm.

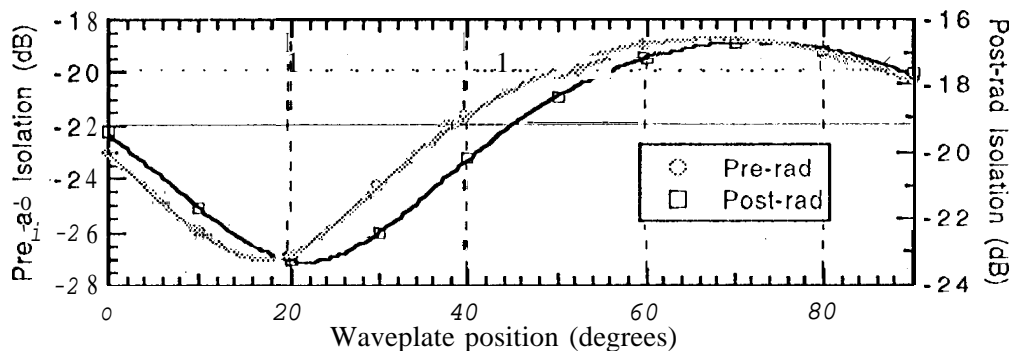
The polarization sensitivity of Gould and ETEK devices were measured before any exposure to radiation and after all irradiations. The variation in isolation as a function of polarization was measured; the peak to peak (p/p) variations in isolation before and after radiation at 1306 nm and 1547 nm are shown in Table 2. The polarization sensitivity was largest for the ETEK device. Since the polarization sensitivity of fused biconical tapered couplers is attributed to the anisotropy of the coupling region [19,20,21], it is suspected that the ETEK device has a less isotropic cross-section in the coupling region. As Table 2 shows, our results indicate that the polarization sensitivity does not change significantly with radiation.

A sample of the data used in peak to peak isolation variations measurements is shown in figure 6. The figure shows pre-rad and post-rad polarization measurements for the ETEK WDM. Like any other birefringent medium, a fused biconical tapered WDM has a sinusoidal dependence on polarization. The variation needs to be periodic since a polarization of 0 degrees is equivalent to a polarization of 180 degrees. Since the polarization is rotated by means of a half-wave plate, the period of the sinusoid is a waveplate rotation of 90 degrees (which corresponds to a rotation in polarization of 180 degrees). The data in

figure 6 is fitted to a sinusoid. The fits are shown as solid lines, and they fit the experimental data very well. Note that the vertical scale is logarithmic, so that a sinusoid of large amplitude (as in fig 6 b) is flatter on the top than on the bottom.



(a)



(b)

Fig. 6 Isolation before and after radiation as a function of waveplate position for E-1. The fits are sinusoidal in dB scale.

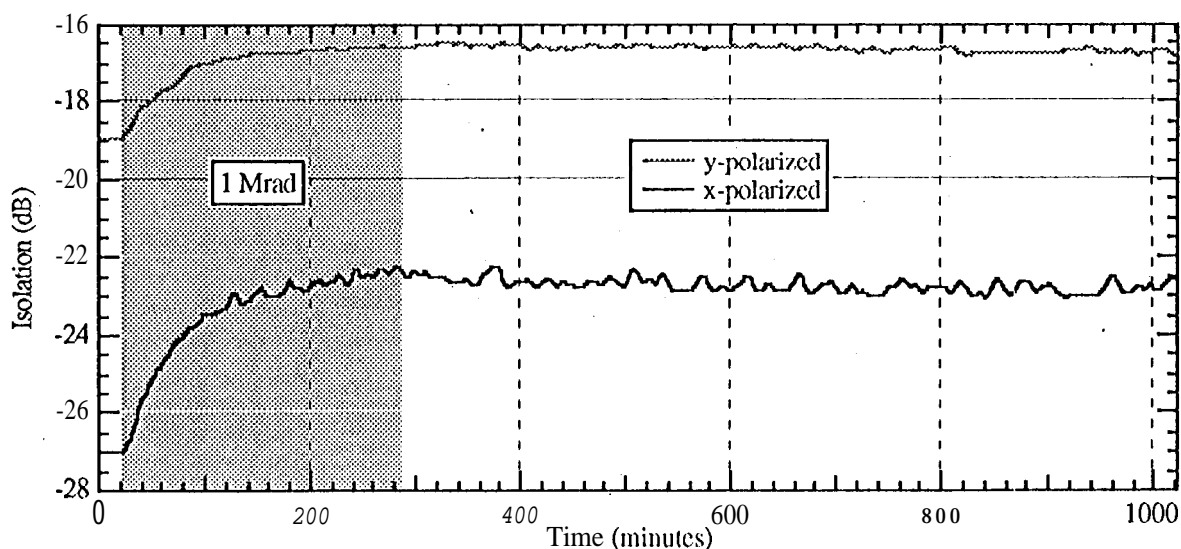


Fig. 7 Isolation changes with radiation (gray area) and relaxation (white area) for E-1 at 1547 nm for x and y polarized light.

The shift in phase of the sinusoids is not a significant effect. In figure 6 a, the measurements were done before and after radiation by reconnecting the fiber. While the fiber at 1547 nm was not moved throughout the experiment, the small phase shift is probably due to the change in the environmentally-induced birefringence of the single mode fiber connecting the polarization control output of the WDM. In order to measure it, radiation results in a phase change, a lot of precautions must be taken, and the experiments presented here were not designed for it.

At 1547 nm, the polarization sensitivity was monitored in-situ by generating plots like the one in figure 6 every minute. The maximum and minimum measured isolations during the entire experiment are shown in figure 7 for 11-1. The maximum in isolation is attributed to x-polarized light and the minimum to y-polarized light. The reason for this will be explained once the theory for these devices has been discussed.

Since environmental changes vary the birefringence of single mode optical fiber, uncontrolled changes in the state of polarization results in increased noise and drift in the isolation of the device. Small changes in the excess loss (<0.2 dB) are also known to be related to changes in polarization, and were measured in these experiments.

4.4. Comparison between Co^{60} and proton irradiations

As table 1 shows, Gould-2 was subjected to consecutive 1 Mrad Co^{60} irradiations. It can be seen from these results that the effect of Co^{60} radiation on saturates. In other words, the effect of each additional Mrad decreases. Table 1 also shows the results consecutive Co^{60} and proton irradiations on M1-2. More than two weeks separated the two irradiations. Nevertheless, at 1306 nm, 500 krad of protons resulted in a larger change in the isolation than the initial 500 krad of Co^{60} . At 1547 nm, 500 krad of protons resulted in a larger change in the isolation of the WDM than the 1 Mrad of Co^{60} . It is apparent, from these results, that the initial Co^{60} irradiation did not saturate the effects of radiation for protons. It may then be that protons cause additional isolation change by means of a different mechanism. It is also possible that the devices tested were different. Future experiments in which successive proton and Co^{60} irradiations are performed on the same device may provide an answer.

5. THEORETICAL ANALYSIS

A variety of explanations for the experimentally observed effects of radiation on fused biconical taper WDMs were investigated. These included the effect of normal mode loss [7], coupling into cladding modes, bulk silica index changes, and core index changes. Order of magnitude calculations have been made for these and other effects, and the only effect that matches our experimental observations qualitatively and in the order of magnitude is change in core index. There are some indications in the literature that nonequivalent index changes may also be of importance in other types of optical directional couplers [11 - 13]. An explanation of the theory is presented in this section. An order of magnitude comparison with our experimental measurements is given in the following sections. More experiments need to be performed in order to determine other effects not considered in this paper that may significantly affect the performance of a fused biconical taper WDM.

5.1. Rationale

Previous measurements on irradiated Ge-doped silica core fiber [1-5] indicate the presence of four types of color centers in irradiated Ge-doped silica. These are the $\text{Ge}(1,2,3)$ and $\text{Ge-E}'$ centers with absorption bands at 281 nm, 213 nm, 240 nm, and 517 nm respectively. By the Kramers-Kronig relation [28], the index of refraction (real part of the susceptibility function) is directly related to the absorption (imaginary part of the susceptibility function), so that the color centers in Ge-doped silica also affect its index of refraction. It can be shown that the index increases for wavelengths greater than the absorption wavelength (normal dispersion) and decreases for wavelengths that are smaller (anomalous dispersion). Therefore, since the absorption wavelengths are in the VUV, radiation will increase the index of the Ge-doped cores in SMF28 fiber at 1310 nm and 1550 nm (IR).

The increase in index in the cores of the fibers will affect the coupling of the fused biconical tapered WDMs studied in this paper. As can be seen in figure 3, the change in index in the cores will affect the antisymmetric mode more than the symmetric mode, since the percentage of the electric field in the core region is greater for the antisymmetric mode. The difference in velocity between the two modes will decrease, changing the phase shift between the two modes at the end of the coupling region. As will be shown in the more detailed analysis that follows, the effect will be a positive shift in wavelength of the isolation vs. wavelength curve.

5.2. Theoretical Model

The most commonly used model for a fused biconical tapered coupler ignores the coupling in the taper regions and approximates the coupling region by a rectangular dielectric waveguide as shown in figure 8.

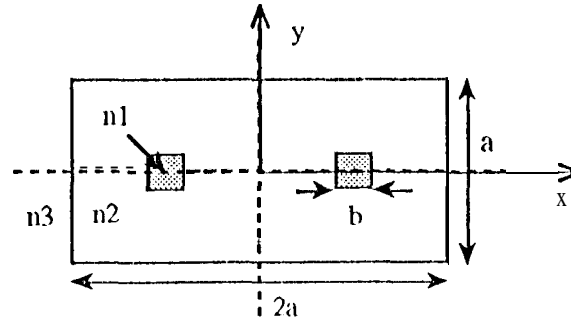


Fig.8 Diagram of the rectangular dielectric waveguide used to model the coupling region of a WDM.

When this simple structure is assumed, the coupling constants for both polarizations can be easily calculated by using equation (3). The coupling constants for x and y polarized modes in the rectangular dielectric waveguide are given from [17] by:

$$C_x + C_y = \frac{3\pi\lambda}{32\pi^2(n_2^2)} \left[\frac{1}{\left(1 + \frac{1}{V}\right)^{22-1}} + \frac{1}{\left(1 + \frac{n_3^2}{n_2^2} \frac{1}{V}\right)^2} \right] \quad (4)$$

$$C_x - C_y = \frac{3\pi\lambda}{16n_2a^2} \cdot \frac{1}{V} \left(1 - \frac{n_3^2}{n_2^2} \right) \quad (5)$$

where n_2 is the index of the cladding, n_3 is the index of the surrounding medium (typically air), a is the height of the rectangular cross section as seen in figure 6, and:

$$V = \frac{2\pi a}{\lambda} (n_2^2 - n_3^2)^{1/2} \quad (6)$$

The analysis resulting in equations (4) and (5) ignores the cores of the fibers. These are shown as shaded squares in figure 6. In order to model the effects of a change in the index of refraction of the core, the effect of core index on the coupling constant needs to be calculated. This will be done by approximating the change in the effective indices of the symmetric and antisymmetric modes with an overlap integral calculation.

Marcattoli solved for the modes of a rectangular dielectric waveguide [27]. We are only concerned about the first (two) fundamental modes which are the $E_{11}^{x,y}$ (symmetric) and $E_{21}^{x,y}$ (antisymmetric) linearly polarized modes. (These two modes are really 'TM' modes with very small electric field in either the x or y direction.) Inside the waveguide, the fields are given by:

$$E_S^{x,y} = E_0 \cdot \cos(k_x^{x,y} x) \cdot \cos(k_y^{x,y} y) \quad (7)$$

$$E_A^{x,y} = E_0 \cdot \sin(2k_x^{x,y} x) \cdot \cos(k_y^{x,y} y) \quad (8)$$

where E_S is the electric field for the symmetric mode and E_A is the electric field for the antisymmetric mode. The superscripts denote the polarization. The functional form of the electric field is independent of polarization, but due to the dependence on polarization of k_x and k_y , the shape of the modes is slightly dependent on polarization.

For x-polarized light:

$$k_x^x = \frac{\pi}{2a} \left(1 + \frac{n_3^2}{n_2^2} \frac{1}{V} \right)^{-1}$$

$$k_y^x = \frac{\pi}{a} \left(1 + 2 \frac{1}{V} \right)^{-1}$$

For y-polarized light:

$$k_x^y = \frac{\pi}{2a} \left(1 + \frac{1}{V} \right)^{-1}$$

$$k_y^y = \frac{\pi}{a} \left(1 + 2 \frac{n_3^2}{n_2^2} \frac{1}{V} \right)^{-1}$$

The effective index of each mode is given by the overlap integral of the square of the electric field and the index of refraction shown in figure 8. Assuming that the mode shape does not change appreciably with the inclusion of the cores, we can approximate the change in the effective index of a mode as follows:

$$\Delta n_{eff} = (n_1 - n_2) \left\{ \frac{\int_{\frac{a-b}{2}}^{\frac{a+b}{2}} dx \int_0^{b/2} dy \cdot |E|^2}{\int_0^a dx \int_0^a dy \cdot |E|^2} \right\} \quad (9)$$

where n_1 is the index of refraction of the core and b is the width of the core in the model shown in figure 8.

Using equations (7), (8) in equation (9), we can calculate the change in the symmetric and antisymmetric indices of refraction caused by the cores of the fibers:

$$\Delta n_S = (n_1 - n_2) \cdot \frac{\left[b + \frac{1}{k_x} \sin k_x b \cos k_x a \right] \left[b + \frac{1}{k_y} \sin k_y b \right]}{\left[a + \frac{1}{k_x} \sin k_x a \cos k_x a \right] \left[a + \frac{1}{k_y} \sin k_y a \right]} \quad (10)$$

$$\Delta n_A = (n_1 - n_2) \cdot \frac{\left[b - \frac{1}{2k_x} \sin 2k_x b \cos 2k_x a \right] \left[b + \frac{1}{k_y} \sin k_y b \right]}{\left[a - \frac{1}{2k_x} \sin 2k_x a \cos 2k_x a \right] \left[a + \frac{1}{k_y} \sin k_y a \right]} \quad (11)$$

We can use equation (3) together with equations (10) and (11) to solve for the change in the coupling constant caused by the difference between the core and cladding indices of refraction. The final result is a correction of equation (4) when the core index is taken into account:

$$C_x + C_y = \frac{3\pi\lambda}{32n_2a^2} \left| \frac{1}{\left(1 + \frac{1}{V}\right)^2} + \frac{1}{\left(1 + \frac{n_3^2}{n_2^2} \cdot \frac{1}{V}\right)^2} \right| + \Delta C_x + \Delta C_y \quad (12)$$

$$C_x - C_y = \frac{3\pi\lambda}{16n_2a^2} \cdot \frac{1}{V} \left(1 - \frac{n_3^2}{n_2^2} \right) + \Delta C_x - \Delta C_y \quad (13)$$

where,

$$\Delta C_{x,y} = \frac{2\pi(n_1 - n_2)}{\lambda} \left[\frac{\left[b + \frac{1}{k_x^{x,y}} \sin k_x^{x,y} b \right] \left[b - \frac{1}{2k_x^{x,y}} \sin 2k_x^{x,y} b \cos 2k_x^{x,y} a \right]}{\left[a + \frac{1}{k_x^{x,y}} \sin k_x^{x,y} a \right] \left[a - \frac{1}{2k_x^{x,y}} \sin 2k_x^{x,y} a \cos 2k_x^{x,y} a \right]} - \frac{\left[b + \frac{1}{k_x^{x,y}} \sin k_x^{x,y} b \cos k_x^{x,y} a \right]}{\left[a + \frac{1}{k_x^{x,y}} \sin k_x^{x,y} a \cos k_x^{x,y} a \right]} \right] \quad (14)$$

6. CHANGE IN INDEX AT 1310 NM AND 1550 NM

We are not aware that any measurements of the core index change in SMF28 fiber have been made for Co⁶⁰ or proton irradiation. These measurements are necessary in order to accurately determine the effects of radiation on isolation suggested by the theory. For order of magnitude calculations, we will approximate the index change from measurements of core index change of Ge-doped fiber exposed to UV radiation.

Land and Russel [5] measured the effects of high intensity UV (488 nm) irradiation on the core index change of Ge-doped fiber. By using a three term Sellmeier expression, Land and Russel calculate an index change of $1.910 \cdot 10^{-4}$ at wavelengths greater than $1 \mu\text{m}$ for a Ge-doped fiber with a radiation induced absorption of the order of 1000 dB/km at 488 nm. Assuming that the absorption by the Ge(1) color center is mostly responsible for attenuation at wavelengths greater than 300 nm, and a Gaussian absorption lineshape for the Ge(1) color center absorption at 281 nm with a linewidth of 1.97 eV [1], it can be shown that an absorption of 1000 dB/km at 488 nm corresponds to an absorption of 12.6 dB/km at 1300 nm. Assuming that the relation between attenuation and index change is the same for UV and Co⁶⁰ irradiations, and since the measured absorption of SMF28 fiber exposed to Co⁶⁰ after a dose of 1 Mrad at 50 degrees Celsius is 13 dB/km [3], we will approximate the core index change for SMF28 fiber to be 10^{-4} /Mrad.

A value of 10^{-4} after 1 Mrad will be used in the next section to compare between the theory and the experimental results. Since many assumptions are made in the calculation of the index change, it is possible that our estimate may be off by as much as an order of magnitude. The authors are aware that a direct measurement of the index change in the core of the fiber for both Co^{60} and proton irradiations is necessary for a true comparison between theory and experimental data.

7. COMPARISON BETWEEN THEORY AND EXPERIMENT

7.1. Red-shift in isolation vs. wavelength

Using equations (12), (13) and (14), in equation (2), the change in the isolation due to a change in the index of the core can be easily calculated. Figure 9 shows the isolation as a function of wavelength near 1550 nm before and after irradiation for x and y polarized light. The numbers used in the calculation are:

$$a = 1.5 \mu\text{m}$$

$$n_3 = 1$$

$$n_2 = 1.458$$

$$b/a = 9/125$$

The length of the coupler was 6.9 mm in order to locate the maximum and minimum coupling near 1310 nm and 1550 nm before radiation. The maximum isolation predicted by the theory is too high since the excitation of higher order modes [23] and the effect of normal mode losses [7] are ignored. This was corrected for in the figure by adding 0.001 to the coupling constant C , thus making the maximum isolation -30 dB. The change in core index caused by the radiation is assumed to be 10^{-4} . According to the model, it can be seen that radiation causes a red-shift in the isolation vs. wavelength curve (see figure 7). This result is in agreement with our experimental observations.

In the experiment, isolation improved in some devices, and degraded in others. As shown in figure 7, if the wavelength of the laser used to test the device is much longer than the wavelength of maximum isolation, a red-shift of the isolation curve will improve the observed isolation. If, on the other hand, the probing wavelength is much shorter than the wavelength of maximum isolation, radiation will degrade the isolation of the WDM. There are some wavelengths for which the isolation first degrades and then improves or vice versa. There are also some wavelengths for which the isolation improves in one polarization and degrades for the other polarization.

The ITTEK device that was tested has a slightly smaller polarization dependence than the theory predicts, but the experimental results agree reasonably well with the changes in isolation shown by the markers between 1.54 μm and 1.55 μm in figure 9. The change in isolation in dB is less for the y-polarized light (dark markers) than for the x-polarized light (light markers). The difference in the initial isolation is also consistent with experiment.

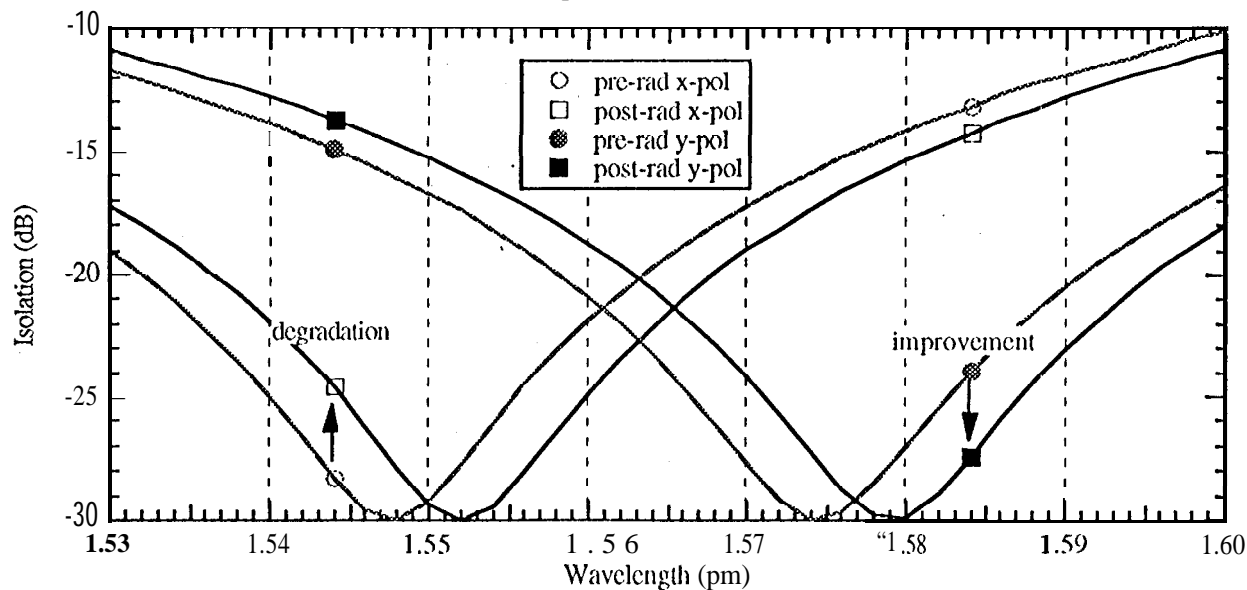


Fig 9. Plot of equation (12) before and after a core index change of 10^{-4} for both x-polarized and y-polarized light.

Figure 9 only shows a portion of the isolation vs. wavelength curve. It can be shown that the isolation is a sinusoidal function of wavelength for fused biconical tapered WDMs with a maximum at near 1310 nm and a minimum near 1551 nm (or vice versa). In order to make some correlation between the relative position of the laser wavelength and the direction of isolation change with radiation, a sinusoidal fit to four data points was used to locate the relative position of the laser wavelength and the maximum isolation wavelength for the Gould WDMs. To do this, a minimum of four data points are needed since there are four variables (the period of the sinusoid, the amplitude at 1310 nm, the amplitude at 1550 nm, and the phase). The results are shown in figure 10. Two of the data points (at 1311 nm and 1553 nm) were given by the manufacturer, and the other two are from our experimental measurements (at 1306 nm and 1547 nm). The fits are not exact since there is a range of error on each data point of approximately 0.3 dB due to the polarization dependence of isolation. Nevertheless, it is seen that the laser wavelength is shorter than the wavelength of maximum isolation for both devices at 1550 nm. A red shift in the isolation would result in a decrease in isolation. Table 1 shows that the isolation decreased for both WDMs after radiation. Gould-2's isolation at 1306 nm improved, and the fit shows that the laser wavelength (the leftmost data point) is to the right of the isolation peak. Gould-3 degraded in isolation at 1306 nm, and the laser wavelength is nearly at the peak of isolation. Such fits were done for all four Gould devices, and the results were consistent with the direction of isolation change in the experiment.

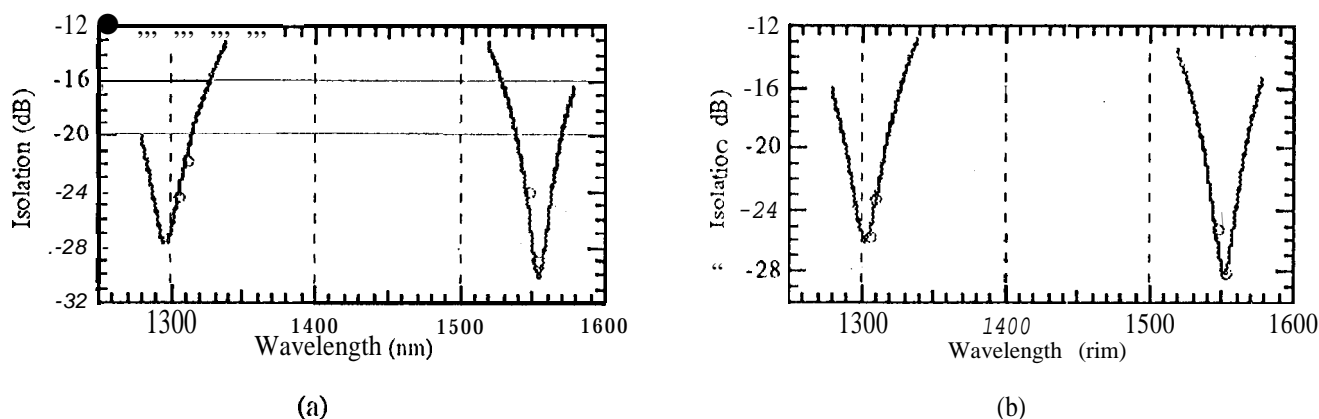


Fig. 10 Sinusoidal fit to pre-rad isolation data for (a) Gould-2 and (b) Gould-3

7.2. Magnitude of wavelength shift

Numerically, the shift in wavelength caused by the change in coupling can also be calculated. As mentioned in section 6, we assume an index change of 10^{-4} for these calculations. Figure 11 shows the dependence of the wavelength shift at 1310 nm on the dimensions of the coupling region. The wavelength shift depends mostly on wavelength and has a very small dependence on polarization. Typical dimensions of these devices range between 15 μm and 20 μm , so the corresponding wavelength shifts range between 5 nm and 10 nm. The shift in wavelength at 1550 nm is 4 nm to 8 nm. If the curves in figure 10 are shifted by 10 nm at 1306 nm and by 8 nm at 1547 nm, it can be seen that post-rad isolation values agree well with the theory.

As can be seen in figure 11, the theory also suggests that a narrower (and thus shorter) WDM may be less sensitive to radiation. This result has not been verified experimentally.

7.3. Sectional irradiations

The results from sectional irradiations on ML-3 and Gould-4 indicate that parts of the taper region are also sensitive to radiation. Even though the taper regions are not included in the theory, this would be expected since there is some coupling between the two fibers in the taper regions. A complete calculation of the coupling in fused biconical tapered couplers may be useful to accurately model the effects of radiation, but such a detailed analysis would not be effective in providing a fundamental understanding of the problem.

7.4. Proton vs. Co^{60}

As was mentioned in section 4.4, it appears that protons may induce a larger index change in these couplers than Co^{60} . Since the present theory does not explain the possible differences, it is possible that there is another mechanism for changing the index of refraction of the cores, unrelated to color center absorption. It has been suggested in the literature [5] that ionizing radiation may form permanent electric dipoles in Ge-doped SiO_2 . The frozen-in electric fields could generate localized

refractive index changes by means of the electro-optic effect. Since protons generate large amounts of electron-hole pairs as they go through the fiber, they may generate larger index changes than Co^{60} irradiation.

Measurements of the polarization sensitivity before and after proton irradiation as well as localized electric field measurements on proton irradiated fiber may provide insights into the physical mechanism responsible for our observations.

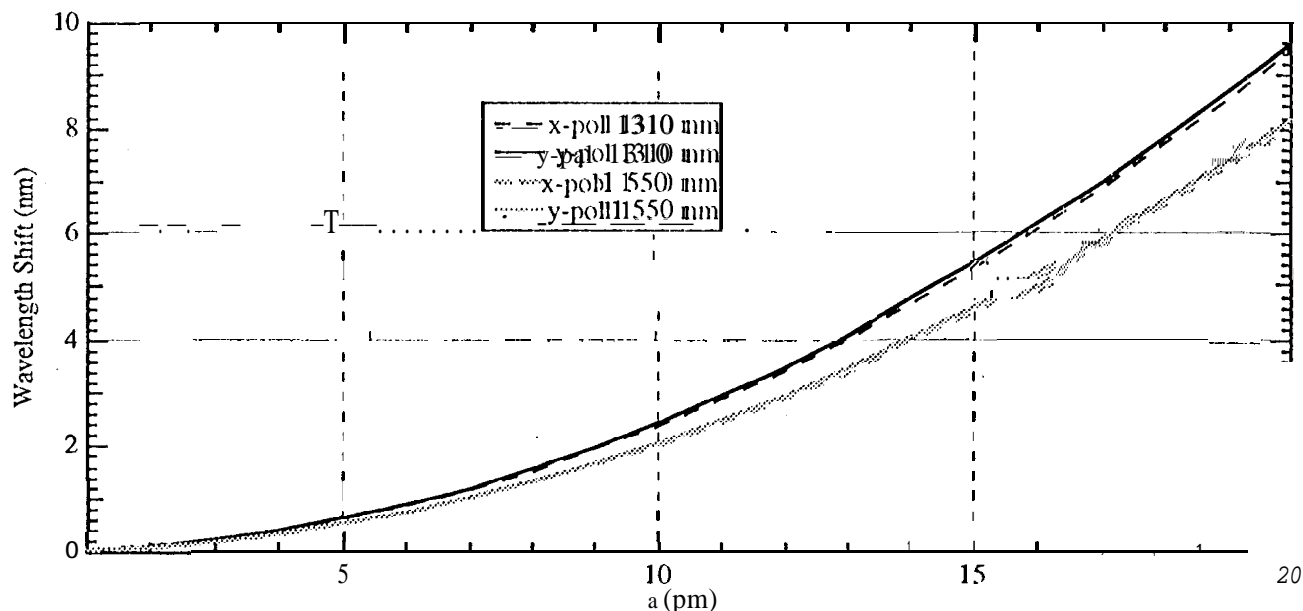


Fig. 11 Dependence of wavelength shift on dimensions of the coupling region for x and y polarized light at 1310 nm and 1550 nm.

8. CONCLUSION

The effects of Co^{60} and proton irradiation of fused biconical taper wavelength division multiplexers for 1310 nm and 1550 nm have been investigated. Changes in the excess loss of these devices is less than 10⁻⁴ dB/krad, while changes in isolation as large as 10⁻² dB/krad were measured. A theoretical model indicates that a core index change of 10⁻⁴ in the fibers used to make a fused biconical taper WDM may result in a red shift in the coupling of the device of nearly 10 nm. It is suspected that a dose of 1 Mrad of Co^{60} or protons may cause index changes in that order of magnitude, thus affecting the isolation of the WDM by amounts consistent with experimental observations. The polarization sensitivity of fused biconical taper WDMs was also investigated before and after radiation. While radiation did not significantly increase the polarization sensitivity of any of the devices tested, it is concluded that polarization must be controlled in some fashion when testing these devices. The radiation sensitivity of different regions of the device was also experimentally investigated. It has been found that the center of these devices is most sensitive to radiation, but that regions around the center are also somewhat sensitive.

Eight separate devices from three different manufacturers were tested in a total of twenty two irradiations. The results from straight irradiations, annealing at room temperature after radiation, and measurements on the effect of polarization on isolation of five WDMs were described. In addition, sectional irradiation measurements on two WDMs and a comparison between proton and Co^{60} were briefly discussed.

If core index changes are primarily responsible for the changes in isolation experimentally observed, our theory suggests that the manufacture of fused biconical taper WDMs may be tailored so that the isolation improves when exposed to radiation. Our theory also suggests that a WDM with a shorter and narrower coupling region may be less sensitive to radiation. These factors may be of considerable importance in the development of a radiation hard fused biconical taper WDM. Other devices that may be similarly affected by radiation include tapered waveguide optical filters, fused biconical taper polarization splitters, and evanescently coupled devices.

The authors wish to thank Simon Cao at E-TEK and Matt McLandrich at NCCOSC for donating devices for the tests described in (his paper,

The research described in this paper was carried out by the Jet Propulsion Laboratory, California Institute of Technology, and sponsored by the National Aeronautics and Space Administration Office of Safety and Mission Assurance (code-QW).

9. REFERENCES

- [1] E.J. Friebele and D. L. Griscom, "Color Centers in Glass Optical Fiber Waveguides", *Mat. Res. Symp. Proc.* **61** (1986)
- [2] V.B. Neustruev et al, "UV and Gamma Induced Colour Centres in Germanium-doped Silica Glass and Fibers", *SPIE 992 Fiber Optics Reliability: Benign and Adverse Environments II* (1988)
- [3] E.J. Friebele, M. Li. Gingerich, and D.L. Griscom, "Survivability of Optical Fibers in Space", *SPIE 1791 Optical Materials and Testing: Benign and Adverse Environments* (1992)
- [4] B. Male, et al, "Ultraviolet light Photosensitivity in Ge-doped Silica Fibers: Wavelength Dependence of the Light-induced Index Change", *Opt. Lett.* **15**, 17 (1990)
- [5] D. P. Hand, and P. St. J. Russell, "Photoinduced Refractive-index Changes in Germanosilicate Fibers", *Opt. Lett.* **15**, 2 (1990)
- [6] Michel Digonnet and H.J. Shaw, "Wavelength multiplexing in single-mode fiber couplers", *Appl. Opt.*, **22**, 3 (1983)
- [7] Robert C. Youngquist, Loren F. Stokes, Herbert J. Shaw, "Effects of Normal Mode Loss in Dielectric Waveguide Directional Couplers and Interferometers", *IEEE J. Quantum Electron.*, **QE-19**, 12 (1983)
- [8] Yariv, Amnon, *Introduction to Optical Electronics*, 3d Ed. New York: Holt Rinehart and Winston Inc., 1985.
- [9] Marcuse, Dietrich, *Theory of Dielectric Optical Waveguides*. New York: Academic Press, 1974.
- [10] H.F. Schlaak, "Modulation Behaviour of Integrated optical Directional Couplers", *J. Opt. Comm.*, **S**, 4 (1984)
- [11] E.W. Taylor, "Radiation Effects in Guided Wave Devices", *SPIE 1794 Integrated optical Circuits II* (1992) pp 54-61
- [12] E. W. Taylor, "Behaviour of Coupled Waveguide Devices in Adverse Environments", *SPIE 1314 Fibre Optics (1990)* pp 155-167
- [13] E. W. Taylor, "Ionization-Induced Refractive index and Polarization Effects in LiNbO₃:Ti Directional Coupler Waveguides", *J. Lightwave Tech.*, **9**, 3 (1991) pp 33S-40
- [14] D.R. Moore, "Reliability Testing of Fused Couplers", *SPIE 988 Components for Fiber Optic Applications and Coherent Lightwave Communications* (1988) pp 27-33
- [15] G. Winzer, "Wavelength Multiplexing Components--A Review of Single-Mode Devices and Their Applications", *J. Lightwave Tech.*, **1:1-2,4** (1984) pp 369-78
- [16] H. Ishio, J. Mioowa, and K. Nosu, "Review and Status of Wavelength-Division-Multiplexing Technology and Its Application", *J. Lightwave Tech.*, **LT-2**, 4 (1984) pp 448-63
- [17] F.P. Payne, C. D. Hussey, and M. S. Yataki, "Polarisation Analysis of Strongly Fused and Weakly Fused Tapered Couplers", *Electron. Lett.*, **21**, 13 (1985) pp 561-3
- [18] A. Ankiewicz, A. W. Snyder, X. H. Zheng, "Coupling Between Parallel Optical Fiber Cores--Critical Examination", *J. Lightwave Tech.*, **LT-4**, 9 (1986) pp 1317-23
- [19] P. P. F'sync, C. D. Hussey, and M. S. Yataki, "Modelling Fused Single-Mode-Fibre Couplers", *Electron. Lett.*, **21**, (1985) pp 461-2
- [20] J. D. Love, M. I. Ian, "Polarisation Modulation in Long Couplers", *Electron. Lett.*, **21**, 12 (1985) pp 519-21
- [21] A. W. Snyder, "Polarising Beamsplitter from Fused-Taper Couplers", *Electron. Lett.*, **21**, 14 (1985) pp. 623-5
- [22] J. V. Wright, "Wavelength Dependence of Fused Couplers", *Electron. Lett.*, **22**, 6 (1986) pp. 320-1
- [23] M. Eissenmann and E. Weidel, "Single-Mode Fused Biconical Couplers for Wavelength Division Multiplexing with Channel Spacing between 100 and 300 nm", *J. Lightwave Tech.*, **6**, 1 (1988) pp 113-9
- [24] H. Henschel, O. Koho, and H. U. Schmidt, "Radiation sensitivity of fibre optic couplers", *SPIE 1791 Optical Materials Reliability and Testing* (1992) pp 151-63
- [25] M. Bertolotti, et al, "Radii and refractive index changes in γ -irradiated optical fibres", *Rad. Effects. Lett.*, **43** (1979) pp 177-80
- [26] V. J. Tekippe, "Passive Fiber Optic Components Made by the Fused Biconical Taper Process", *SPIE 1085 Optical Fibers and Their Applications* (1990)
- [27] E. A. J. Marcetili, "Dielectric Rectangular Waveguide and Directional Coupler for Integrated Optics", *Bell Sys. Tech. J.*, **48**, (1969) pp. 2071-2102
- [28] Yariv, Amnon, *Quantum Electronics* 3d Ed., New York: John Wiley & Sons, Inc., 1989